Electronic Supplementary Material (ESI) for Nanoscale.

Supporting Information

Improved Performance of $SrFe_{12}O_{19}$ Bulk Magnets through Bottom-Up Nanostructuring

*Matilde Saura-Múzquiz,[1] Cecilia Granados-Miralles,[1] Marian Stingaciu,[1] Espen Drath Bøjesen,[1] Qiang Li,[2] Jie Song,[2] Mingdong Dong,[2] Espen Eikeland[1] and Mogens Christensen[1]**

[1] Center for Materials Crystallography, Department of Chemistry and Interdisciplinary Nanoscience Center (iNANO), Aarhus University, Langelandsgade 140, 8000 Aarhus C, Denmark

[2] Center for Nanotechnology (CDNA), Interdisciplinary Nanoscience Center (iNANO), Aarhus University, Gustav Wieds Vej 14, 8000 Aarhus C Denmark

*e-mail address of corresponding author: mch@chem.au.dk

Demagnetizing factor *N*. Experimental calculation.

When a magnetic material is magnetized by an external magnetic field, a so called demagnetizing field, H_d, with opposite direction to that of the magnetization, *M*, will appear due to the magnetic free poles created on the magnetic material's ends. The intensity of the demagnetizing field is proportional to the density of the magnetic free poles, and to a shape-dependent factor, *N*, called demagnetizing factor.[1]

$$H_d = N \cdot M$$

The demagnetizing factor *N* is generally represented by a symmetric 3 × 3 matrix, and can be easily deduced for simple shapes like a sphere (*N*=0.33), a long needle with the magnetization along the axis (*N*=0) or perpendicular to it (*N*=0.5), or a thin film with the magnetization in plane (*N*=0) or out of plane (*N*=1).

The calculation of *N*, however, becomes more complex in the case of less simple shapes, or polycrystalline samples, where *N* is dependent on the shape of the particles (as long as they are single domain)[2], the shape of the measured sample, the packing density and the degree of crystallite orientation. It is therefore highly complex to determine the theoretical value of *N* for our samples, where the platelet-like shape of the crystallites, the cylindrical shape of the measured sample, the density and the crystallite orientation play an important role. For this reason, and in order to make the magnetic results easily comparable, an approximation of *N*=0.33 was used for all the samples

As an alternative, an experimental approximation can be performed graphically for the SPS samples, given the squareness of their hysteresis loops. The experimentally calculated *N* value corresponds to that one at which the magnetization around the coercive field is closest to follow a vertical line. For a perfectly square hysteresis, that would correspond to the *N* at which the derivative of the magnetization around the coercive field is equal to infinite. This experimental calculation is not possible to carry out for the powder samples, as they do not present square hysteresis curves, and therefore the graphic approximation becomes un-trustworthy. Given the random orientation of the nanoplatelets in the powder samples, we find the approximation of N=0.33 to be the most appropriate one, assuming isotropic samples.

The experimental calculation of *N* for the three SPS samples is shown in Figure S 1. In dashed lines, the hysteresis curves with a demagnetizing factor of 0.33 are shown for each sample, together with the hysteresis in solid line, corrected by the experimentally found *N* value. For each sample, the experimental *N* is obtained graphically by varying *N* such that the magnetization around H_c is the closest possible to a vertical line, crossing it at H_c. A vertical line at the H_c value of each sample is shown in green in Figure S 1.

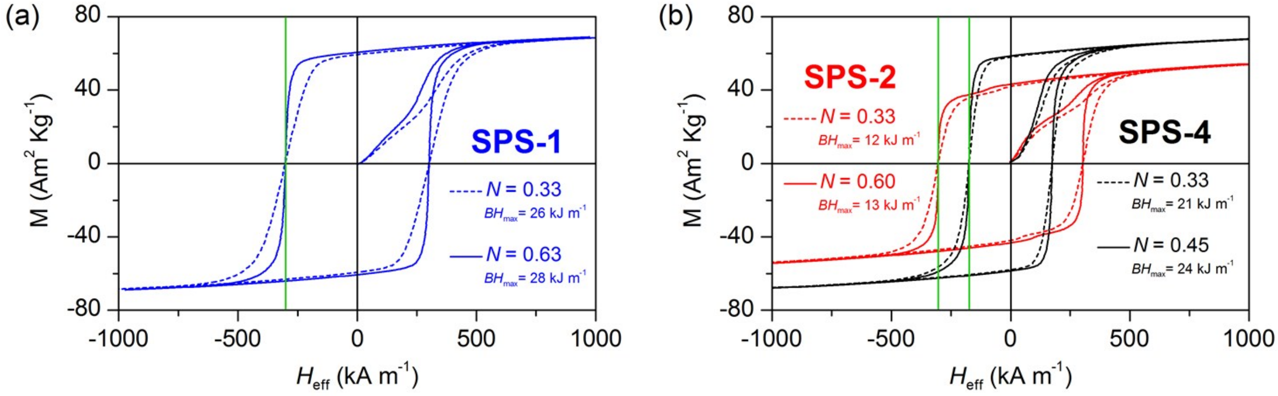

Figure S1: (a) Magnetic hysteresis curves (Magnetization, *M*, vs. Effective Field, H_{eff}) of sample SPS-1. In dashed line, corrected with a demagnetizing factor *N* of 0.33, and in solid line, the experimentally corrected hysteresis of *N* equal to 0.63. A green vertical line is position at H_{eff}=H_c in order to determine *N* experimentally.(b) Magnetic hysteresis curves (Magnetization, *M*, vs. Effective Field, H_{eff}) of samples SPS-2 (in red) and SPS-4 (in black). In dashed lines, corrected with a demagnetizing factor *N* of 0.33, and in solid lines, the experimentally corrected hysteresis curves of *N* equal to 0.60 for SPS12 and 0.45 for SPS14. A green vertical line is position at H_{eff}=H_c in order to determine *N* experimentally.

The maximum energy product is highly dependent on the demagnetizing correction, and it therefore varies upon variation of *N*. The experimentally obtained *N* values, N_{exp}, and the corresponding maximum energy products, BH_{max} for N_{exp}, are given in Table S1, together with comparison with the obtained BH_{max} for N=0.33.

Table S1: Experimental demagnetizing factor, N_{exp}, obtained graphically for the three SPS samples, BH_{max} attained with demagnetizing correction by N_{exp} and comparison with the BH_{max} attained with N=0.33.

Sample	N_{exp}	BH_{max} [kJ m^{-3}] for N_{exp}	BH_{max} [kJ m^{-3}] for N=0.33
SPS-1	0.63	28	26
SPS-2	0.60	13	12
SPS-4	0.45	24	21

Details on the Rietveld refinements of X-ray diffraction data

Due to anisotropic shape of the $SrFe_{12}O_{19}$ and FeOOH crystallites, these were modeled as platelets using the Platelets Vector Size model along the *c*-axis,[3] by specifying the vector (001) in *Fullprof Suite*. Thermal parameters and atomic positions were kept fixed, while the zero point offset, background, scale factor, unit cell parameters and Lorentzian peak profile parameters related to size, (Y) and (α_z), were refined. For the measurements performed on the Rikagu SmartLab diffractometer, the instrumental parameters were extracted from a profile matching with constant scale factor of a NIST LaB_6 660b standard. For data collected at SPring-8 synchrotron, a NIST CeO2 standard was used. The standards were measured in the same conditions as the corresponding samples.

1. *Powder Samples – Bimodal size refinement of $SrFe_{12}O_{19}$*

The refined values for volume fraction, crystallite size and unit cell parameters for all the powder samples are given, as well as reliability factors and goodness of fit, χ^2.

For those samples where a bimodal size distribution of $SrFe_{12}O_{19}$ crystallites was employed in the model (FLOW-1 and FLOW-2), refined values for both, unimodal and bimodal models are given as a comparison. An image of the Rietveld refinement of the two different models of samples FLOW-2, were the largest percentage of $SrFe_{12}O_{19}$ – II is observed, is shown in Figure S 2.

FLOW-1	Phase	Volume Fraction (%)	Crystallite Size (nm)		Unit Cell Parameters (Å)		R_f	R_{wp}	X^2
			a-axis	*c-axis*	a=b	c			
Unimodal	$SrFe_{12}O_{19}$ - I	88(1)	32.1(4)	2.97(3)	5.8879(1)	23.114(3)	3.96	15.2	**4.70**
	FeOOH	12(1)	15(2)	6(4)	2.9408(4)	9.347(4)	4.34		
Bimodal	$SrFe_{12}O_{19}$ - I	86(1)	30.2(4)	2.66(3)	5.8887(1)	23.101(4)	3.74	14.5	**4.35**
	$SrFe_{12}O_{19}$ - II	3(1)	Out of res.	38(4)	5.8833(3)	23.136(4)	6.56		
	FeOOH	11(1)	18(2)	6.4(6)	2.9386(4)	9.361(4)	4.65		

FLOW-2	Phase	Volume Fraction (%)	Crystallite Size (nm)		Unit Cell Parameters (Å)		R_f	R_{wp}	X^2
			a-axis	*c-axis*	a=b	c			
Unimodal	$SrFe_{12}O_{19}$ - I	75(1)	40.8(6)	5.47(5)	5.8832(1)	23.098(2)	3.92	17.1	**6.22**
	FeOOH	26(2)	26(2)	1.33(7)	2.9502(1)	9.06(2)	2.28		
Bimodal	$SrFe_{12}O_{19}$ - I	66(1)	29.7(5)	2.67(6)	5.8919(1)	23.062(5)	3.36	12.9	**3.64**
	$SrFe_{12}O_{19}$ - II	20(1)	Out of res.	20.9(7)	5.8828(1)	23.119(1)	4.69		
	FeOOH	14(1)	24(2)	3.6(2)	2.9359(2)	9.071(7)	2.42		

FLOW-4	Phase	Volume Fraction (%)	Crystallite Size (nm)		Unit Cell Parameters (Å)		R_f	R_{wp}	X^2
			a-axis	*c-axis*	a=b	c			
Unimodal	$SrFe_{12}O_{19}$	49(1)	80(1)	27.3(3)	5.88216(6)	23.0928(4)	4.58	12.0	**5.12**
	FeOOH	51(1)	17.0(5)	5.1(1)	2.93350(9)	9.298(1)	3.90		

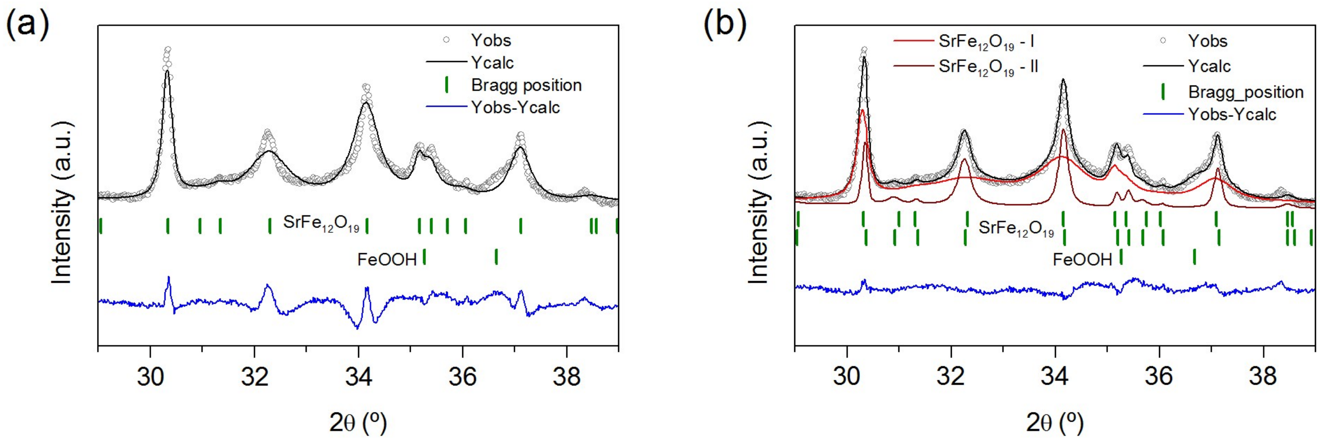

Figure S 2: (a) Refinement of FLOW-2 using the unimodal model. The grey dots are the experimental data, the black line is the calculated model, the green lines are the Bragg positions and the blue line is the difference between the observed and calculated intensities. (b) Refinement of FLOW-2 using the bimodal model. The two refined $SrFe_{12}O_{19}$ phases, I and II, are plotted in red and wine lines respectively, and the overall model in black.

2. *SPS pellets*

The refined values for volume fraction, crystallite size and unit cell parameters for all the SPS samples are given below, as well as reliability factors and goodness of fit, χ^2. The diffraction patter and Rietveld refinement of the three crushed-SPS samples is also shown together with the numeric values obtained from the refinements. In all cases, the black circles are the experimental data, the red line is the calculated model, the blue line is the difference between the observed and calculated intensities, and the vertical lines are the positions of the Bragg peaks for the different phases.

SPS-1

Phase	Volume Fraction (%)	Crystallite Size (nm)		Unit Cell Parameters (Å)		R_f	R_{wp}	X^2
		a-axis	*c-axis*	a=b	c			
$SrFe_{12}O_{19}$	100	102(2)	81(2)	5.88053(4)	23.0557(2)	3.79	10.2	**25.2**

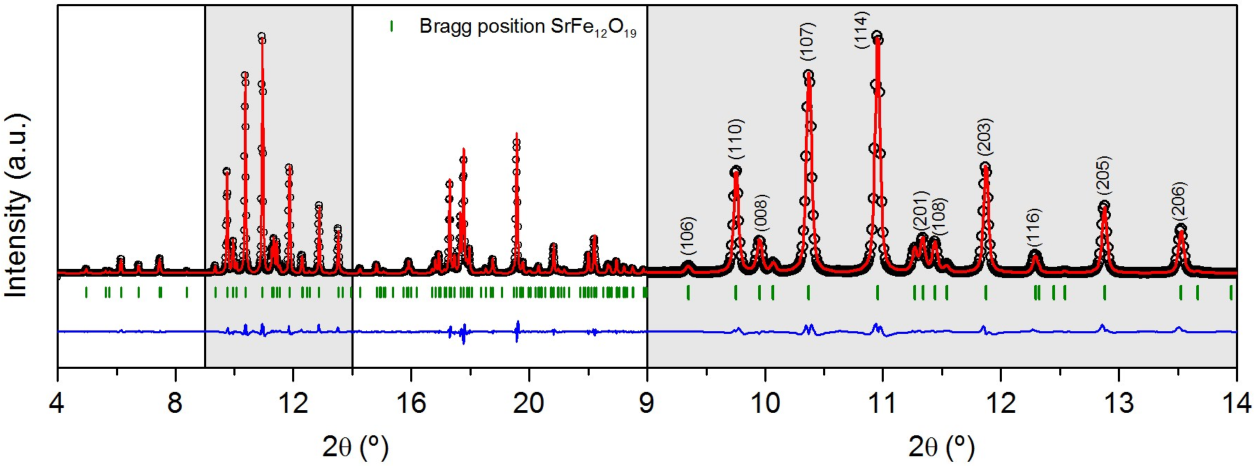

Figure S 3: Rietveld refinement of the powder X-ray diffraction data from the crushed SPS-1 pellet, collected at SPring-8 synchrotron (λ = 0.5000 Å), and magnification of a 2θ region were the main peaks of the phase are indexed.

SPS-2

Phase	Volume Fraction (%)	Crystallite Size (nm)		Unit Cell Parameters (Å)		R_f	R_{wp}	X^2
		a-axis	*c-axis*	a=b	c			
$SrFe_{12}O_{19}$	80.0(3)	109(2)	72(2)	5.88151(4)	23.0535(2)	6.50	13.7	**30.1**
α-Fe_2O_3	20.0(2)	95(2)	95(2)	5.03650(6)	13.7422(2)	5.14		

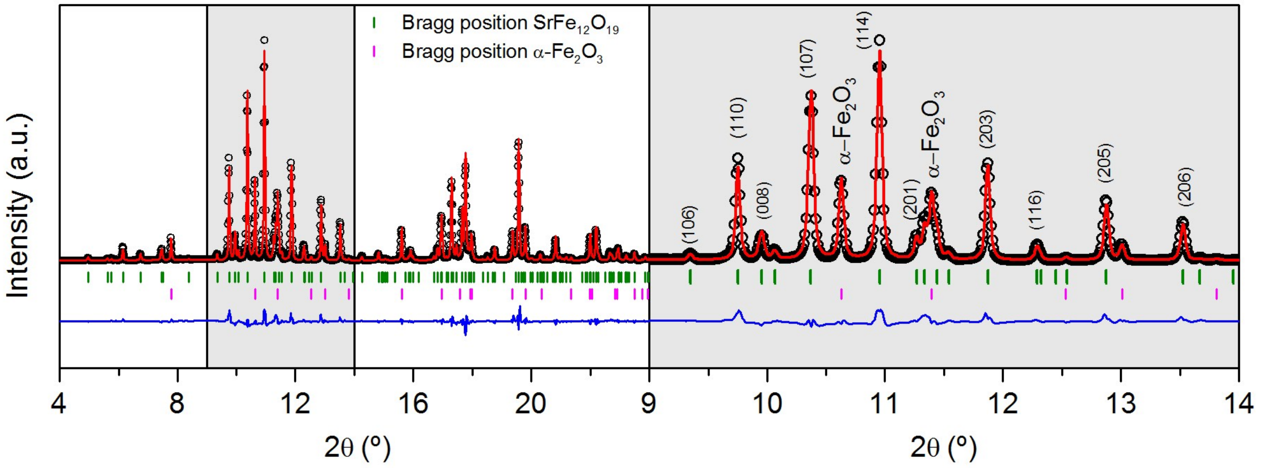

Figure S 4: Rietveld refinement of the powder X-ray diffraction data from the crushed SPS-2 pellet, collected at SPring-8 synchrotron (λ = 0.5000 Å), and magnification of a 2θ region were the main peaks of the phase are indexed, and the main peaks of the impurity phase, α-Fe_2O_3, are marked.

SPS-4

Phase	Volume Fraction (%)	Crystallite Size (nm)		Unit Cell Parameters (Å)		R_f	R_{wp}	X^2
		a-axis	*c-axis*	a=b	c			
$SrFe_{12}O_{19}$	95.4(2)	81.6(8)	53.1(7)	5.88035(3)	23.0622(1)	11.6	12.0	**11.7**
γ-Fe_2O_3	4.6(1)	88(4)	88(4)	8.3958(1)	8.3958(1)	10.2		

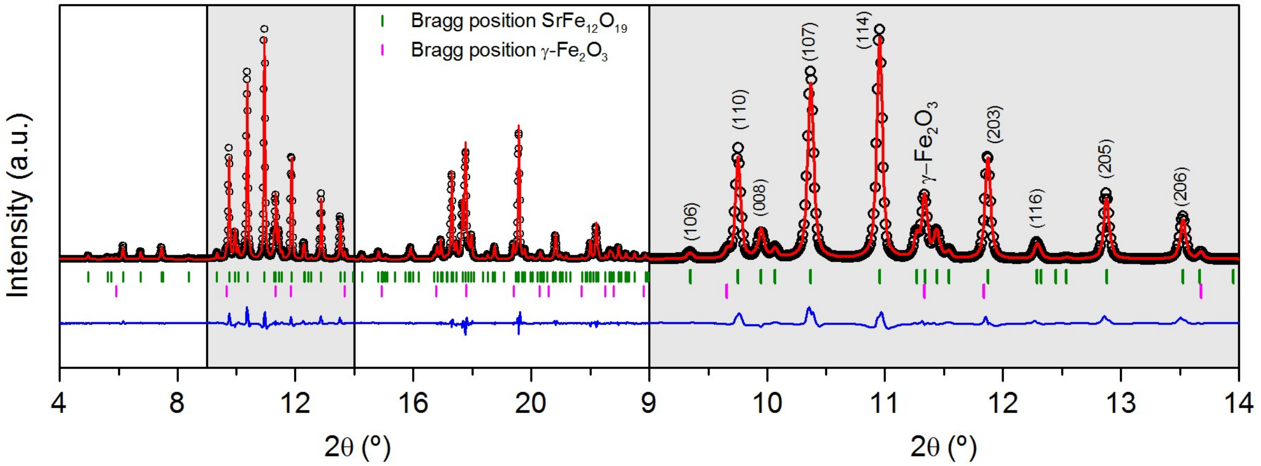

Figure S 5: Rietveld refinement of the powder X-ray diffraction data from the crushed SPS-4 pellet, collected at SPring-8 synchrotron (λ = 0.5000 Å), and magnification of a 2θ region were the main peaks of the phase are indexed and the main peaks of the impurity phase, γ-Fe_2O_3, are marked.

References

1. S. Chikazumi and C. D. Graham, *Physics of ferromagnetism*, Oxford University Press, Oxford New York, 2nd edn., 1997.
2. J. M. D. Coey, *Magnetism and magnetic materials*, Cambridge University Press, Cambridge, 2010.
3. C. Greaves, *J Appl Crystallogr*, 1985, **18**, 48-50.